Regional sea level trend budget over 2004-2022

Marie Bouih[1], Anne Barnoud[1], Chunxue Yang[2], Andrea Storto[2],

Alejandro Blazquez[3] , William Llovel[4], Robin Fraudeau[1] and Anny Cazenave[3]

1. Magellium, 31520 Ramonville St Agne, France

2. Institute of Marine Science, National Research Council of Italy, Rome, Italy

3. Université de Toulouse, LEGOS (CNES/CNRS/IRD/UT3), 31401 Toulouse, Cedex, France

4. Univ Brest, CNRS, Ifremer, IRD, Laboratoire d'Océanographie Physique et Spatiale (LOPS), IUEM, F29280, Plouzané, France

Ocean Science

Second revision, 24 April 2025

Corresponding author : Anny Cazenave

anny.cazenave@univ-tlse3.fr; anny.cazenave@gmail.com

ORCID 0000-0002-2289-1858

ABSTRACT

Closure of the regional sea level trend budget is investigated over the 2004-2022 time span by comparing trend patterns from the satellite altimetry-based sea level with the sum of contributions, i.e. the thermosteric, halosteric, manometric and GRD (Gravitational, Rotational, and Deformational fingerprints due to past and ongoing land ice melt) components. The thermosteric and halosteric components are based on Argo data (down to 2000m). For the manometric component, two approaches are considered: one using GRACE/GRACE-Follow On satellite gravimetry data, and the other using ocean reanalyses-based sterodynamic sea level data corrected for local steric effects. For the latter, six different ocean reanalyses are considered, including two reanalyses that do not assimilate satellite altimetry data. The results show significantly high residuals in the North Atlantic for both approaches. In a few other regions, small-scale residuals of smaller amplitude are observed and attributed to the finer resolution of altimetry data compared to the coarser resolution of data sets used for the components. The observed strong residual signal in the North Atlantic points to Argo-based salinity errors in this region. However, it is not excluded that other factors also contribute to the reported non-closure of the budget in this area.

1. Introduction

On interannual to decadal time scales, sea level changes in a specific oceanic region arise from several factors. The global mean geocentric sea level rise is primarily driven by ocean warming, land ice melting, and water exchange with continents. Additionally, local and regional effects contribute, including changes in seawater density caused by variations in temperature and salinity (steric effects), as well as the redistribution of ocean water mass through circulation changes (manometric component, Gregory et al., 2019), and variations in atmospheric loading. Furthermore, changes in the solid Earth's gravity, rotation, and deformation (GRD) occur in response to mass redistributions from past and present-day land ice melt and land water storage changes. These GRD factors include two components : the Glacial Isostatic Adjustment (GIA) effect, which stems from the last deglaciation, and GRD fingerprints, which are associated with contemporary land ice melting and, to a lesser extent, changes in land water storage (Gregory et al., 2019).

In terms of global average, the rate of sea level rise is dominated by ocean warming via thermal expansion of seawater, and land ice melting (from glaciers, Greenland and Antarctica ice sheets), in response to global warming (e.g., Cazenave et al., 2018, Nerem et al., 2018, IPCC, 2019, 2021, Cazenave and Moreira, 2022, Horwath et al., 2022, Llovel et al., 2023). The spatial variations of the rate of sea level rise mainly result from steric effects, with the thermosteric contribution being generally dominant (e.g., Stammer et al., 2013, Hamlington et al., 2020), except in the Arctic where the halosteric effect is important (e.g., Carret et al., 2017, Tajouri et al., 2024).

Focusing on trends, many studies have computed the global mean sea level budget over the altimetry era (i.e., since the early 1990s) by comparing the global mean sea level rise with the sum of the thermal and mass components from independent observing systems (e.g., Dieng et al., 2017, Nerem et al., 2018, WCRP, 2018, Horwath et al., 2022, Chen et al., 2018, 2020, Barnoud et al., 2021, 2023, to focus only on the most recent publications). These studies have shown that at least until 2016, the global mean sea level budget is closed within the data uncertainties. In recent years, some discrepancy has been observed between the altimetry-based global mean sea level and the sum of the Argo-based steric and gravimetry-based mass components (e.g., Chen et al., 2020, Barnoud et al., 2021, 2023, Mu et al., 2024), especially when using the Gravity Recovery And Climate Experiment (GRACE) and GRACE Follow-On (GRACE-FO) satellite data to estimate the total mass contribution to sea level change, instead of individual mass contributions (i.e., glaciers, Greenland and Antarctica ice sheets, land

waters and atmosphere water vapor). At regional scale, the closure of the sea level budget has been less studied so far. A few recent studies have assessed the closure of the sea level budget at ocean basin-scales, over the altimetry era (e.g., Rietbrock et al., 2016, Frederiske et al., 2016, 2018, 2020; Hamlington et al., 2020, Royston et al., 2020, Camargo et al., 2023, Mu et al., 2024). The regional ocean mass budget has also been investigated (Ludwigsen et al., 2024). Closure of the regional budget is only observed in some regions but not everywhere. For example, using altimetry, gravimetry and Argo data over 2005-2015, Royston et al. (2020) concluded that the regional budget cannot be closed in the Indian-South Pacific region. Similarly, Camargo et al. (2023) also found non-closure of the regional sea level budget in a number of oceanic areas. Using machine learning techniques, these authors were able to identify processes not well captured by the observations that are considered to assess closure of the regional sea level budget.

In the above studies, closure of the regional budget was assessed by averaging the data either at ocean basin-scale or smaller ~~scale~~. In the present study, we revisit the regional sea level trend budget over the GRACE/Argo era (starting in 2004) at the local scale, without averaging the data at the basin-scale. After removing the global mean trend of each component, we focus on the spatial trend patterns, with a resolution of about 300 km, as allowed by the gridded data sets considered, an approach not applied in the previous studies. This approach avoids compensation of spurious positive/negative sub-basin trend patterns and allows for more precise identification of the areas where the sea level trend budget is not closed.

For this investigation, we use gridded satellite altimetry data for the observed sea level changes and Argo data to estimate the thermosteric and halosteric sea level changes. For the manometric component, two types of data are considered: satellite gravimetry data from the GRACE and GRACE FO missions as well as ocean reanalyses to estimate the redistribution of water mass in the ocean (following the same approach as in Camargo et al., 2023, i.e., estimating sterodynamic sea level changes corrected for local steric effects; see section 3). The study period covers the period from January 2004 to December 2022 (although some data sets end in December 2019; section 3).

2. Brief overview of the sea level components at regional scale

2.1. Steric component

The steric component includes the effects of ocean temperature and salinity changes. Remote surface wind forcing, heat and freshwater fluxes associated with variations in the overlying atmospheric state are the two main forcing mechanisms causing steric changes (Stammer et al., 2013, Roberts et al., 2016). Wind forcing modifies the ocean circulation which further redistributes heat and water masses. It is the dominant mechanism of interannual to decadal steric changes in many regions, particularly in the tropics (e.g., Timmermann et al., 2010; Merrifield and Maltrud, 2011; Piecuch and Ponte, 2014; England et al., 2014). Wind forcing can also play a role in the extra tropics and at high latitudes (Roberts et al., 2016). Buoyancy forcing, i.e. surface air-sea fluxes of heat and freshwater (due to surface warming and cooling of the ocean, and exchange of freshwater with the atmosphere and land through evaporation, precipitation, and runoff) is important in mid to high latitudes, e.g., in the North Atlantic Ocean (Gulf Stream and North Atlantic subpolar gyre) (Roberts et al., 2016).

Over the altimetry era, regional sea level patterns are dominated by steric changes. In most regions, the thermosteric component by far dominates the halosteric one, except in the North Atlantic Ocean (Llovel and Lee, 2015) and in high latitude areas, e.g., in the northeast Pacific, and particularly in the Arctic (e.g., Carret et al., 2016; Ludwigsen et al., 2022, Tajouri et al., 2024). On interannual to multidecadal time scales, the spatial trend patterns in (thermo) steric sea level are still largely influenced by basin-scale internal climate modes of variability, e.g., El Niño-Southern Oscillation (ENSO), Pacific Decadal Oscillation (PDO), Atlantic Multidecadal Oscillation (AMO), North Atlantic Oscillation (NAO) and Indian Ocean Dipole (IOD). Wind stress changes on such time scales are indeed directly related to climate modes (Han et al., 2017). For example, sea level in the tropical Pacific oscillates from west to east with ENSO (with high/low sea level in the eastern/western part during El Niño/La Niña events), in response to wind-forced propagating waves. In the North Atlantic, surface wind and heat flux partly drive interannual to decadal sea level fluctuations and are associated with the NAO (but changes in the Atlantic Meridional Ocean Circulation also contribute) (Han et al., 2017). In the tropical Indian Ocean, interannual to decadal variability in sea level is strongly influenced by ENSO and the IOD (Han et al., 2017, 2019).

2.2. Manometric component

The total manometric sea level change has two components: (1) the total water mass added to the ocean (the latter being called barystatic component) due to land ice melt and to the exchange of water with the continents, and (2) the spatial redistribution of water mass by the ocean circulation (Gregory et al., 2019). Added water to the oceans due to the ~~The~~ global mean barystatic contribution nearly uniformly covers the oceanic domain rapidly (within a few weeks) via a barotropic global adjustment occurring on short time scales (Lorbacher et al., 2012). Because the global mean trend of each component of the regional sea level budget is removed in this study, the barystatic component (i.e., the global mean ocean mass change) disappears. Compared to steric changes, the manometric sea level change due to water mass redistribution (barystatic contribution removed), plays a smaller role on interannual to decadal time scales, but can be sizeable (e.g., Dangendorf et al., 2021, Wang et al., 2022), in particular at high latitudes and over shallow continental shelves (e.g., Forget and Ponte, 2015; Carret et al., 2021).

2.3. Atmospheric loading

On seasonal and longer time scales, sea level responds as an inverted barometer to atmospheric loading (Wunsch and Stammer, 1997) i.e. the sea surface height increases (decreases) by 1 cm if the local surface pressure decreases (increases) by approximately 1 mbar. The atmospheric loading component is quite small compared to the thermosteric one, but it is non-negligible at high latitudes (e.g., in the Arctic Ocean where it can reach 0.3 mm/yr equivalent sea level on interannual to decadal time scales, Proshutinski, 2004). Atmospheric loading can be estimated using e.g. surface pressure data from atmospheric reanalyses.

2.4. Gravity, Earth Rotation, and solid Earth Deformations (GRD)

The response of the solid Earth to past and present-day water mass exchange between continents and oceans causes global and regional sea level changes. The GIA results from the ice and water mass redistribution of the last deglaciation. Its effect depends on the Earth's mantle viscosity and deglaciation history. The response of the solid Earth to ongoing land ice melt essentially depends on the elasticity of the lithosphere and mantle, as well as on the amount and location of ice mass loss. These mass redistributions induce changes in the gravity, rotation, and visco-elastic deformations of the solid Earth (Mitrovica et al., 2001, Milne et al., 2009, Stammer et al., 2013). These are the so-called GRD (Gravity, Earth Rotation, and solid Earth Deformations) fingerprints (Gregory et al., 2019). In the literature,

the GRD contribution is often separated into the one resulting from the GIA (last deglaciation) and the contemporary GRD effects, the latter referring to mass redistributions due to present-day land ice melt and land water storage variations. In terms of global average, the GIA effect on the absolute sea level change is around -0.3 mm/yr (Peltier, 2004; Tamisiea, 2011, Caron et al., 2018). Its regional signature is mostly uniform, except in formerly glaciated high-latitude regions. The contemporary GRD fingerprints produce complex regional patterns : sea level drops near the melting bodies but sea level rises in the far field (e.g., along the northeast coast of North America). Several studies have theoretically computed the impact of contemporary GRD changes on relative and absolute sea levels, by solving the sea level equation, either assuming a priori current ice sheet mass loss (e.g., Mitrovica et al., 2001, Tamisiea, 2011, Spada, 2017), or using realistic ice mass loss based on observations from the GRACE satellite gravimetry mission (Adhikari et al., 2019). Note that the sea level fingerprints associated with the GIA and the contemporary GRDs are usually expressed in terms of linear trends and have a small amplitude (<0.5 mm/yr except around the ice sheets where the magnitude increases to ~1 mm/yr), compared to the observed regional sea level and steric sea level trends of several mm/yr magnitude. However, with the expected increase of land ice melt in the coming decades, the contribution of the contemporary GRD fingerprints to regional sea level trends may become increasingly significant.

3. Data and methods

3.1. Data

3.1.1 Altimetry-based total sea level

Total sea level is routinely observed by satellite altimetry. In this study, we use the daily 1/4° x 1/4° gridded sea level anomaly data version DT2021 from the Copernicus Climate Change Service (C3S) (https://climate.copernicus.eu). To ensure the long-term stability of this altimetry-based data, C3S sea level anomalies rely on two simultaneous satellite missions at any given time: the successive reference missions (TOPEX/Poseidon, Jason-1, Jason-2, Jason-3, and Sentinel-6 Michael Freilich) plus an auxiliary mission from the global constellation. The dataset is corrected for TOPEX-A altimeter drift (Ablain et al., 2017), as well as for the Jason-3 radiometer drift that impacts the wet troposphere correction (Brown et al., 2023). The dataset covers the period from January 1993 to December 2023. The C3S dataset is corrected for GIA using the ICE6G-D model (Peltier et al., 2018). The uncertainty in the rate of the global mean sea level is estimated to be 0.3 mm/yr (Ablain et al.,2019, Guérou et al.,

2023). At regional scale, trend uncertainties are larger, on the order of 1 mm/yr especially in coastal areas (Prandi et al., 2021).

3.1.2 Steric sea level

We compute the Argo-based steric sea level data from the Roemmich-Gilson Argo climatology of the Scripps Institution of Oceanography (SIO) which provides monthly gridded data of temperature T and salinity S at a 1° x 1° resolution and 58 depth levels until 2000 meters (Roemmich and Gilson, 2009) (data downloaded in July 2024). The choice for the SIO product is motivated by the fact that its post-processing corrects for the salinity drift reported in Argo floats since 2015, which misleads to a spurious increase reported in the global mean salinity (Wong et al., 2023, Liu et al., 2020, 2024, Ponte et al., 2021). This salinity drift has a significant impact on the sea level budget closure (Chen et al., 2020, Barnoud et al., 2021). The SIO processing methodology considers the most up-to-date delayed-mode Argo profiles which have been meticulously quality-controlled by a scientist (typically within 1-2 years after the float transmits the data). In addition, the SIO processing adjusts the real-time Argo profiles (which have passed through automatic quality-control typically within 24 h) to fit the WOCE (World Ocean Circulation Experiment) global hydrographic climatology. This specific processing has the benefit of removing the salinity drift in the SIO steric sea level data (Liu et al., 2024). The dataset covers the period from January 2004 to December 2022, within the 0–2000 m depth range, and the latitudes between 66°S and 66°N.

In this study, the deep ocean's contribution to steric sea level is not considered due to its small magnitude (on the order of 0.1 mm/yr) and possibly high uncertainty (e.g., Purkey and Johnson, 2010). Based on deep Argo profiles, Lele and Purkey (2024) estimated the deep ocean steric sea level rise (temperature and salinity contribution) being 0.13 ± 0.16 mm/yr in the south Pacific Ocean over 2014-2023, confirming the small contribution of the deep steric sea level rise.

The thermosteric, halosteric and total steric sea level changes are computed from the gridded temperature and salinity data using the Lenapy library (https://github.com/CNES/lenapy) from the Centre National d'Études Spatiales (CNES), based on the Gibbs seawater oceanography toolbox of the 2010 Thermodynamic Equation Of Seawater (TEOS-10).

3.1.3 Manometric sea level

The manometric sea level change is estimated using two independent methods.

The first approach relies on satellite gravimetry data from the GRACE mission (2002-2017, Tapley et al., 2019) and GRACE-FO mission (launched in 2018, Landerer et al., 2020), which enables to estimate changes in the Earth's gravitational field linked to mass redistribution,

including the regional sea level variations due to GRD effects. Two kinds of GRACE solutions are considered:

- (1) An ensemble mean of so-called mass concentration (mascon) solutions (update from Blazquez et al., 2018). We use the latest GRACE and GRACE-FO Release 6 mascon solutions from the Center for Space Research (CSR; Save et al., 2016), Jet Propulsion Laboratory (JPL; Watkins et al., 2015), and Goddard Space Flight Center (GSFC; Loomis et al., 2019). These mascon solutions are corrected for the GIA effect using the ICE6G-D model (Peltier et al., 2018), as well as for the geocenter motion using the correction from Sun et al. (2016). The effects of the ocean dynamics and atmospheric loading are restored using the GAD product derived from the Atmosphere-Ocean Dealiasing (AOD1B) models (Flechtner et al., 2015, Dobslaw et al., 2017). To retrieve the ocean mass contribution comparable to the difference between altimetry and Argo, the effect of the mean atmospheric pressure over the ocean is removed using the spatial mean of the GAD product at each month (Chen et al., 2019). The manometric component is estimated as the mean of these three gridded ocean mass products, which are given in equivalent water height.
- (2) An ensemble of 60 spherical harmonic (SH) solutions. This ensemble is derived from the manometric GRACE-based products (DOI: 10.24400/527896/a01-2023.011 version 4.0) and distributed at AVISO+ (https://aviso.altimetry.fr). This product allows for uncertainty estimates linked to various stages of GRACE and GRACE-FO data processing (Blazquez et al, 2018). This ensemble of 60 solutions results from the combination of five processing centres, three C20/C30 (spherical harmonics of degree 2 and 3 of the gravity field potential) estimates, two GIA models (ICE6G-D from Peltier et al., 2018 and the model from Caron et al., 2018), and two levels of denoising and decorrelation kernel filtering. The geocenter motion is corrected with a model based on the approach developed by Sun et al. (2016) and Swenson et al. (2008). Each ensemble member is also corrected for the water vapor mass in the atmosphere using the C0 from GAA (Chen et al, 2019). For each ensemble member, atmospheric loading over the ocean is restored using the GAD products (Flechtner et al., 2015, Dobslaw et al., 2017) to correct for the inverse barometer effect, aligning the ocean mass variations with satellite altimetry data in which atmospheric loading is already accounted for.

The two sets of GRACE solutions used here cover the period from January 2004 to December 2022. In case of missing monthly data, a linear interpolation is applied to account for the data gaps. However, no interpolation is performed for the ~one-year gap between GRACE and GRACE-FO.

The second approach follows Camargo et al. (2023) method which derives the manometric sea level change from ocean reanalyses. Ocean models provide the sterodynamic sea level change, i.e., the sea level change due to changes in ocean density and circulation, with the inverse barometer correction applied (Gregory et al., 2019; Storto et al., 2024). The corresponding manometric component is derived by subtracting the local steric effect from~~to~~ the reanalysis-based sterodynamic sea level, and adding the contemporary GRD fingerprints (Gregory et al., 2019; Camargo et al., 2023). It is the approach followed here.

We consider six different ocean reanalyses with different characteristics as listed in Table 1. GLORYS, C-GLORS, ORAS5, and FOAM use the NEMO (Nucleus for European Modelling of the Ocean) ocean model and assimilate satellite altimetry-based sea level data. The SODA reanalysis is based on the MOM (Modular Ocean Model) developed by NOAA (National Oceanographic and Atmospheric Administration, USA) and does not include altimetry data. All reanalyses have a spatial resolution of 0.25°. In order to assess the regional sea level budget with another manometric component independent of satellite altimetry data, we also consider an ensemble reanalysis at lower resolution and without altimetry data assimilation (called CIGAR; see Table 1). This variety of reanalyses offers the opportunity to evaluate the degree of consistency of the manometric signal from reanalysis-based products.

Table 1: Characteristics of the six ocean reanalyses used in this study to estimate the manometric sea level change patterns independently from GRACE and GRACE-FO data.

Reanalysis	Ocean model, Spatial Resolution, End date	Data assimilation of altimetry-based sea level data	References
GLORYS (MOI)	NEMO, 0.25°, 2022	Yes	Garric and Parrent (2017)
C-GLORS (CMCC)	NEMO, 0.25°, 2022	Yes	Storto and Masina (2016)
ORAS5 (ECMWF)	NEMO, 0.25°, 2022	Yes	Zuo et al. (2019)
FOAM (UK Metoffice)	NEMO, 0.25°, 2022	Yes	Blockley et al. (2014)
SODA (Version	MOM4, 0.25°,	No	Carton et al. (2018)

3.4.2, U. Maryland)	2019		
CIGAR (CNR-ISMAR)	NEMO, 1°, 2022	No	Storto and Yang (2024)

To compare the manometric component derived from ocean reanalyses with the one based on GRACE and GRACE-FO, we added the contemporary GRD contribution to the reanalysis-based manometric sea level change. We used the sea level fingerprint data from Adhikari et al. (2019), which provides monthly contemporary GRD fingerprints at a 0.5° x 0.5° resolution. Because the Adhikari et al. (2019) data set ends in 2016, we linearly extrapolated the GRD fingerprints up to 2022 and added the corresponding trends to the ocean reanalyses-based manometric trends.

3.2. Method

Systematic corrections for both atmospheric loading and GIA effects are applied to altimetry-based and satellite gravimetry datasets, even though different models are used in each dataset. The MOG2D (Carrere and Lyard, 2003) and inverse barometer model is used for altimetry data (www.aviso.altimetry.fr), while the GAD product is used for GRACE and GRACE-FO data (see section 3.1.3). Likewise, the GIA corrections rely on the ICE6-G model for altimetry (Peltier et al. 2018), while GRACE datasets use either ICE6-G (Peltier et al. 2018) or Caron et al. (2018) model.

All datasets were spatially interpolated onto a 1° x 1° grid and were averaged on a monthly basis. For spatial consistency, a common masking technique was applied to all gridded components. This mask covers latitudes from 66°S to 66°N, excludes inland seas, and omits coastal regions where the distance from land is less than 300 km.

All datasets span from January 2004 to December 2022, except for the oceanic reanalyses-based manometric components for which two study periods were considered, depending on the dataset availability: January 2004-December 2019 and January 2004-December 2022.

Finally, seasonal signals (annual and semi-annual) were removed at each grid mesh of each data set through a simple least-squares adjustment of 6-month and 12-month sinusoids, and a 3-month Lanczos filter was applied locally to each dataset to remove high frequency signals. The global mean trend of each dataset computed over the study period was also removed before constructing the spatial trend maps.

For each gridded data set, we computed a trend uncertainty map.
For the altimetry data, we used the trend uncertainties provided by Prandi et al. (2021). These are based on a statistical computation which estimates via a generalized least-squares approach the total uncertainty of regional sea level trends due to all sources of errors affecting the altimetry-based sea level measurements (i.e., orbit, range, geophysical corrections and intermission bias). In this approach, individual variance-covariance matrices describing time correlated errors are computed for each source of uncertainty. Uncertainties from all sources are further combined by summing up the variances. Regional sea level trend uncertainties provided by Prandi et al. (2021) with this method, applied to altimetry-based sea level grids of 2°x2° resolution over 1993-2019 are on the order of 1 mm/yr or less (1-sigma). The largest errors are located along the continental coastlines.
Since the SIO temperature and salinity data are not provided with uncertainties, we computed trend uncertainties for the thermosteric and halosteric components by considering the dispersion between two thermosteric/halosteric monthly data ~~products~~ with respect to their mean: the SIO product used here and the EN4 T/S database, version 2.2 (https://www.metoffice.gov.uk/hadobs/en4/download-en4-2-2; Good et al., 2013). We estimated the thermosteric and halosteric trend uncertainty at each grid mesh from the dispersion between the two data sets (SIO and EN4) around the mean. For the total steric, thermosteric and halosteric trend uncertainties were quadratically combined.

As the ensemble mean of the 60 SH GRACE solutions is provided with trend uncertainties, (adapted from Blazquez et al., 2018), these are used here for both GRACE-based manometric components (i.e., the ensemble mean mascon and the SH solutions).

Finally, for the uncertainties of the residual trend map (based on GRACE for the manometric component), we quadratically combined trend uncertainties of all components at each grid mesh.

Please note that the reanalyses used here do not provide uncertainty estimates.

In Figure S1 of the Supplementary Information (SI) are shown trend and associated trend uncertainty maps for the altimetry-based sea level, components and residuals. Note that for altimetry-based sea level and components, the trend uncertainty map includes the global mean trend uncertainty (of smaller magnitude than the regional trends). Uncertainties correspond to 1-sigma errors.

4. Results: Regional sea level trend budget with GRACE and Argo

4.1. Trend patterns in observed sea level, components and residuals

Figure 1 shows the maps of altimetry-based sea level trends, of the GRACE- and Argo-based component trends, and of the residual trends (i.e., trend differences between altimetry-based sea level and sum of components). Hatched areas on the figures correspond to regions where the signal to noise ratio is not significant. This is based on comparing at each grid mesh, the observed trend with the trend uncertainty (shown in Figure S1). From Figure 1, we note that except for the elongated negative pattern east of the Philippines in the western tropical Pacific, the altimetry-based sea level trends are significant everywhere. Concerning the GRACE-based manometric component, trends are not significant over a large portion of the northeast Atlantic. The halosteric map displays a few regions where the trends are not significant. Most are located in the southern hemisphere. Accordingly, these translate into the total steric map. Finally, the residual trend map shows that the signal is significant essentially in areas where the residual trends are positive. Over several hatched areas, the residual trends are not significantly different from zero. This concerns most of the Pacific Ocean and a portion of the South Atlantic Ocean.

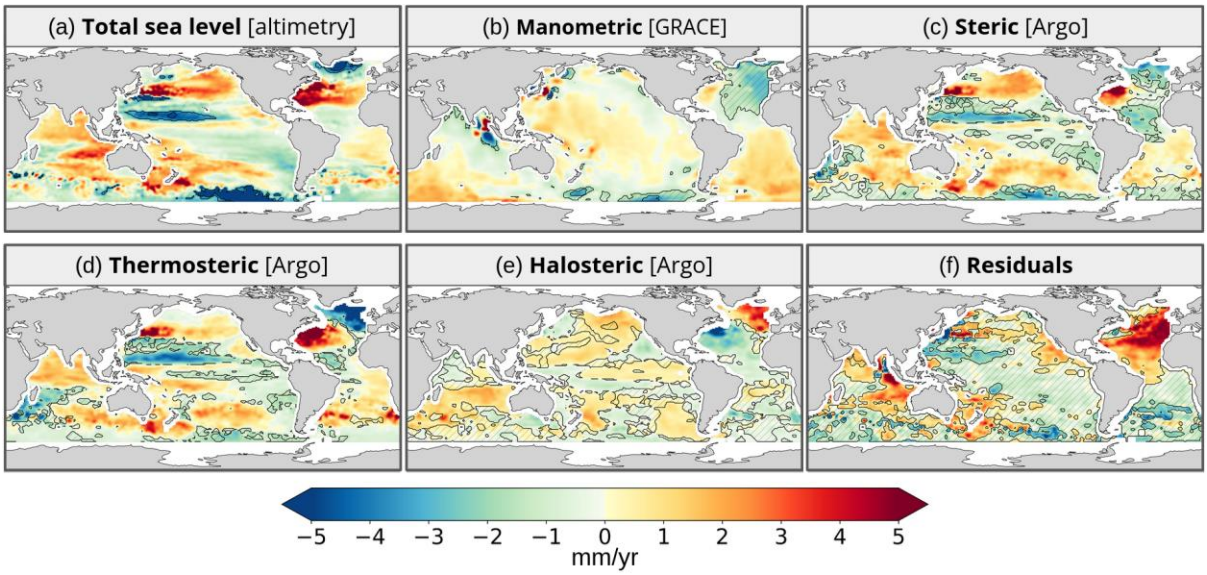

Figure 1: Sea level trends over January 2004 to December 2022 in total altimetry-based sea level (a), manometric component based on GRACE mascons (b), Argo-based total steric (c), thermosteric and halosteric components (d and e) and budget residual trends (observed sea level minus sum of components) (f). The hatched areas correspond to regions where the signal trend value is not significant compared to the corresponding trend uncertainties.

Visual inspection of Figure 1 confirms earlier findings, i.e., the observed regional trend patterns are dominated by the thermosteric trend patterns (as expected; e.g., Stammer et al., 2013; Hamlington et al., 2020; Cazenave and Moreira, 2022). In the North Atlantic, thermosteric and halosteric trends have opposite signs. Except for two spots of high signal along the coasts of north Indonesia and Japan due to the solid Earth response to the Sumatra and Tohoku earthquakes in 2004 and 2011 respectively (not removed here), the manometric trend map is dominated by large-scale patterns, positive over almost the whole Pacific, as well as over the south Atlantic Ocean and southwest Indian Ocean. The absence of small-scale patterns likely results from the lower resolution of GRACE and Argo data compared to other data sets.

The residual trend map shows that in many regions, the sum of components cancels out the observed trends. This is the case over most of the Pacific Ocean, part of the South Atlantic Ocean and southwest Indian Ocean. In these regions, the residuals are not significantly different from zero, which suggests that the regional sea level budget can be considered as closed.

In the eastern Indian Ocean, along the coast of North Indonesia, the positive residuals are related ~~result from the solid Earth signal due~~ to the 2004 Sumatra earthquake~~, not removed from the GRACE-based manometric component.~~ The same is true for the positive residuals east of Japan and associated with the 2011 Tohoku earthquake. Besides these two regions, it is in the North Atlantic Ocean that the strongest positive residual trends are observed. In this region, altimetry-based and thermosteric sea level displays positive trends in the western part and negative trends south of Greenland while opposite patterns are seen in the halosteric component. The strong residual signal in the North Atlantic is discussed in detail in section 6.

4.2. GRACE data assessment

In this section, we explore the impact of the geocenter and GIA corrections applied to GRACE data on the residual trend map, considering that these two corrections remain imperfectly

known (Blazquez et al., 2018). For that purpose, we decomposed the sea level budget components into spherical harmonics and computed the residuals for various configurations of low degree harmonics (see Figure S2 and Table S1 in the Supplementary Information, SI). Figure S2 and Table S1 show that degree 1,0 (related to the geocenter motion) and degree 2,1 (related to polar motion and GIA correction) harmonics contribute to the high positive residuals observed in the North Atlantic Ocean.

GRACE data are classically corrected for the geocenter motion when compared with altimetry data, in order to mov~~e~~ing GRACE observations from the centre of mass to the centre of figure of the reference system, in which the altimetry-based sea level is supposed to be also expressed after correcting the satellite orbits for the geocenter motion (Alexandre Couhert, personal communication).

Using the ensemble of 60 spherical harmonic solutions described in Section 3.1, we constructed an alternative ensemble of 60 solutions without applying the correction for the geocenter motion, i.e. keeping the GRACE observations in the center of mass reference system. Comparing these two ensembles of solutions allows us to assess the influence of the geocenter correction on the manometric component and, consequently, on the residuals of the sea level budget. Figure 2 shows the impact of the geocenter correction on the manometric trends as well as on the associated residual trends. Not correcting for the geocenter motion reduces the residuals observed in the North Atlantic Ocean but increases the residual trends elsewhere, with larger residuals in almost all other ocean basins. Thus, even if the Sun et al. (2016)'s geocenter correction may not be optimal, it minimizes the residual trend~~s~~, except in the northeast Atlantic Ocean.

Let's remind that GRACE data are classically corrected for the geocenter motion when compared with altimetry data, in order to mov~~e~~ing GRACE observations from the centre of mass to the centre of figure of the reference system, in which the altimetry-based sea level is supposed to be also expressed after correcting the satellite orbits for the geocenter motion (Alexandre Couhert, personal communication). ~~This questions the actual referential of altimetry data and the consistency of the processing between satellite altimetry and satellite gravimetry data. Normally, this should be consistent as altimetry-based sea level is supposed to be expressed in a center of figure reference frame, like the GRACE data after correcting for the geocenter term. However, the way the geocenter is corrected in the orbits used in the altimetry-based processing could still be an issue (Alexandre Couhert, personal communication).~~ ~~Besides, if~~ If no geocenter correction is applied, the GRACE-based manometric component displays large scale signals not observed by altimetry data, so that the corresponding residual trends (Figure 2d) also present unrealistic large-scale signals.

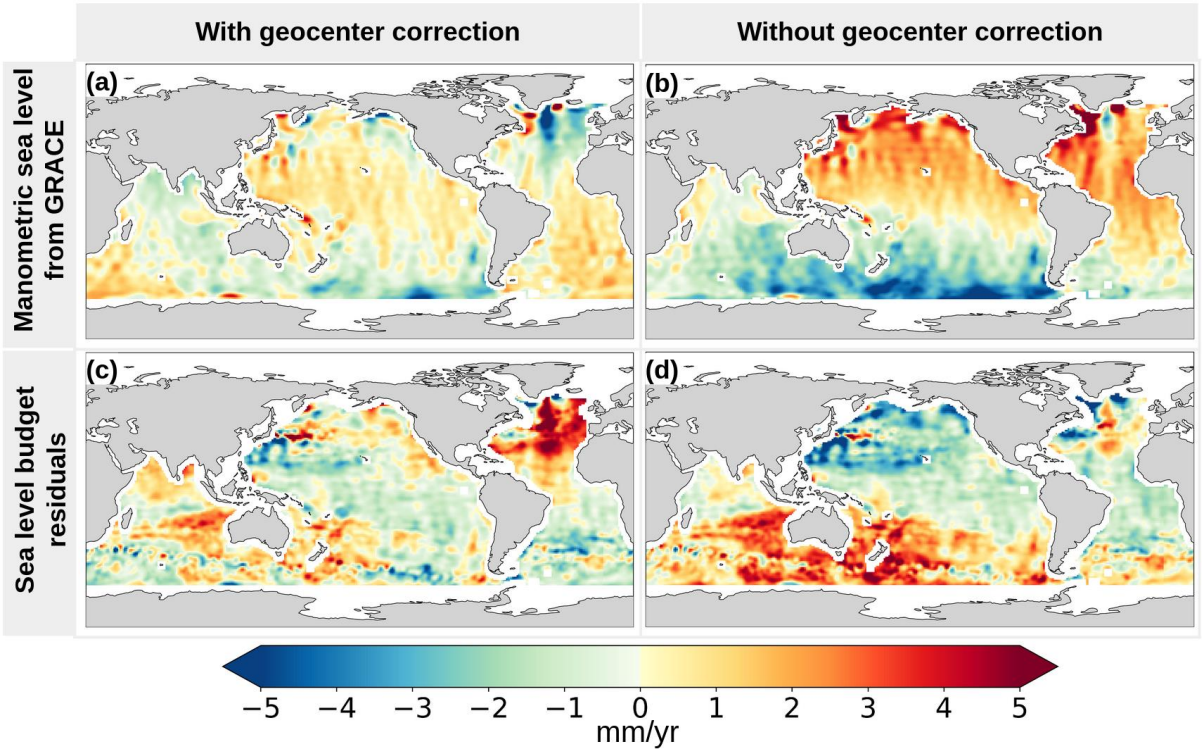

Figure 2: Sea level trends of GRACE-based manometric component and corresponding budget residuals with and without the geocenter correction. (a) Manometric sea level trend map with the geocenter correction, (b) Manometric sea level trend map without the geocenter correction, (c) Sea level budget residual trend map computed with the manometric component corrected for the geocenter, (d) Sea level budget residual trend map computed with the manometric component not corrected for the geocenter.

To estimate the impact of the GIA corrections on the manometric component and budget residuals, we further formed two separate subsets of 30 solutions each, for each GIA model (Peltier et al, 2018 and Caron et al., 2018), applying the Sun et al. (2016)'s geocenter correction to each subset. Unlike for the geocenter case, no significant difference was observed.

5. Regional sea level trend budget using ocean reanalyses for the manometric component

As explained in section 2, according to Gregory et al. (2019) and Camargo et al. (2023), the dynamic ocean mass redistribution due to ocean circulation changes can be estimated from the sterodynamic sea level corrected for local steric changes. Thus, in this study, we apply

463 Camargo et al. (2023)'s approach and use ocean reanalyses to estimate the manometric
464 component, in order to further assess closure of the regional sea level budget.

465 As detailed above (section 3), six different ocean reanalyses have been considered over their
466 common period from January 2004 to December 2019. However, to compute the ensemble
467 mean reanalysis, we discarded FOAM because of its spurious trends in the South Atlantic and
468 South Indian Ocean. Figure 3 shows the reanalysis-based manometric trend maps over 2004-
469 2019, for each of the six data sets, as well as the ensemble mean based on CIGAR, C-
470 GLORS, GLORYS, ORAS5 and SODA. The manometric components based on the two sets
471 of GRACE solutions, restricted to this study period, are also shown.

472 No uncertainties are provided with the reanalyses data so that it is not possible to highlight the
473 areas where the signal is significant for the individual cases (Figure 3a-d). This can be done
474 however for the ensemble mean (Figure 3g) where the errors are estimated from the
475 dispersion of the five reanalyses (CIGAR, C-GLORS, GLORYS, ORAS5 and SODA) about
476 the mean.

477

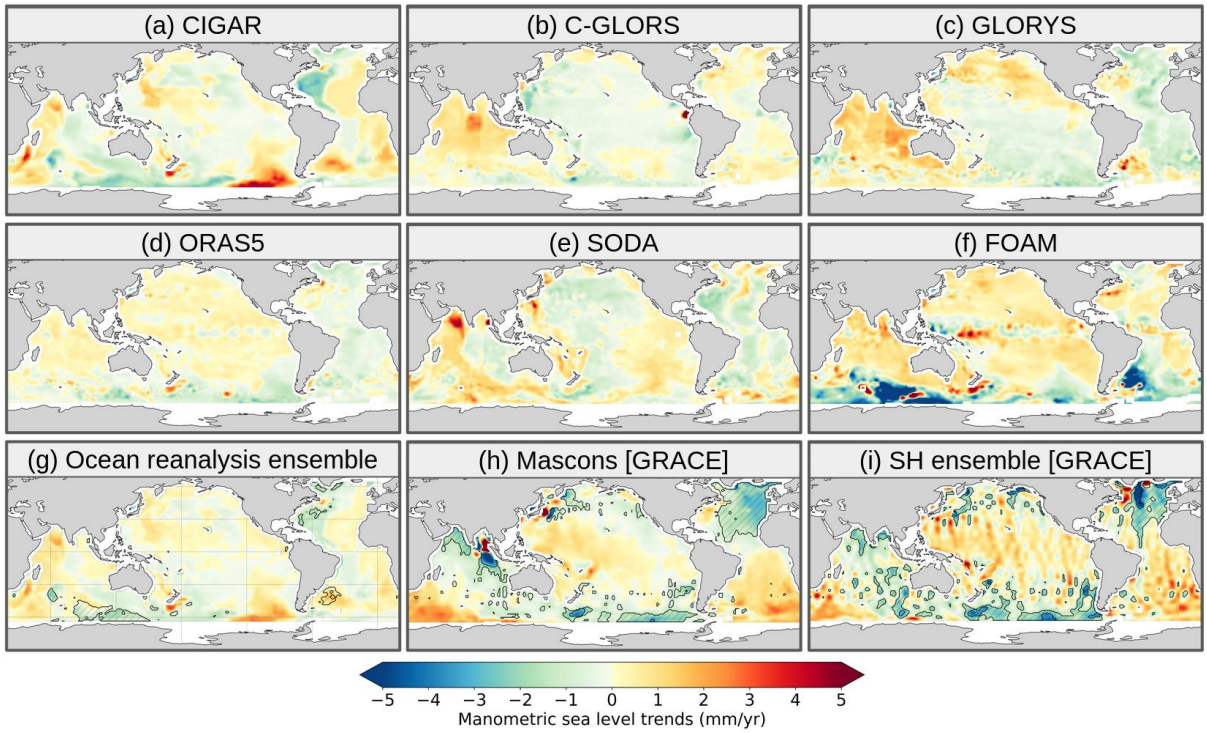

478

479 *Figure 3 : Reanalysis-based manometric trend maps over January 2004-December*
480 *2019 for each of the six ocean reanalyses: CIGAR, C-GLORS, GLORYS, ORAS5,*
481 *SODA and FOAM (panels a to f). Panel (g) shows the ensemble mean of the five*
482 *reanalyses (CIGAR, C-GLORS, GLORYS, ORAS5 and SODA). Panels h and i refer*
483 *to the manometric component from the GRACE mascon and GRACE spherical*

harmonic (SH) ensembles. Hatched areas in panels 3g, 3h, 3i represent regions where the signal is not significant.

The six reanalyses provide quite different manometric trend patterns. The FOAM and ORAS5 patterns are quite similar in the Pacific and Indian Oceans. In these regions, C-GLORS, CIGAR and GLORYS show rough agreement. SODA's patterns differ from the other reanalyses everywhere, although they look similar to CIGAR in the Indian Ocean. As mentioned above, the FOAM-based manometric map shows spurious high trends in the South Atlantic and South Indian Ocean. This is why it is not included in the ensemble mean.

Comparing ensemble mean reanalyses-based manometric map with the GRACE-based manometric maps, we note that : (1) the spatial patterns of the reanalysis-based manometric trend map have generally slightly lower amplitude than the GRACE ones in many regions, except around Antarctica, and (2) the manometric spatial trends of the ensemble mean reanalyses and GRACE have opposite signs in many regions, including in the North Atlantic.

The regional trend budget has been computed with each of the six reanalyses as well as for the ensemble mean (FOAM excluded), all other data being kept unchanged. The corresponding residual trend patterns are shown in Figure 4 .

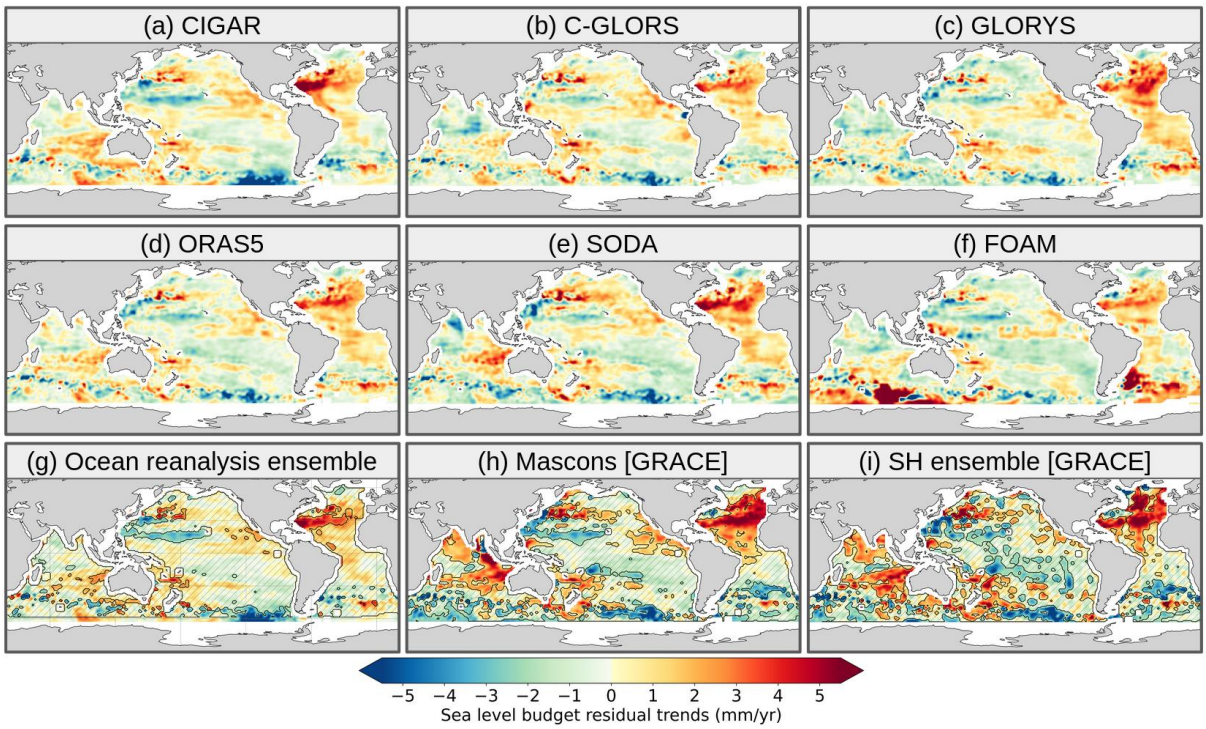

Figure 4: Residual trends of the regional sea level budget computed with each of the six reanalyses-based manometric components, as well as with the ensemble mean (FOAM excluded) (panels a to g) (with altimetry-based and steric components unchanged). GRACE-based residual trends for both mascon and spherical harmonic solutions are also shown (panels h and i). The period of analysis here is from January 2004 to December 2019. Hatched areas in panels 4g, 4h, 4i represent regions where the signal is not significant.

The CIGAR, C-GLORS, SODA, ORAS5, and GLORYS reanalyses give very similar residual trend patterns, even though SODA uses completely different ocean model and data assimilation schemes, and no altimetry-based sea level data are assimilated. Note that CIGAR also does not assimilate altimetry-based sea level anomaly data, but it is forced by the latest atmospheric reanalysis from ECMWF (unlike the other reanalyses) and embeds a daily varying runoff dataset for freshwater discharge into the oceans. Again, one outlier is FOAM which shows strong positive residual trends in the Southern Atlantic and South Indian Ocean. The ensemble mean residual trend map (FOAM excluded) displays slightly lower signal than the GRACE cases (compare panel 4g with panels 4h and 4i in Figure 4). What is striking is that the two approaches (reanalyses and GRACE) show positive residual trends in the North Atlantic. However, the residuals are significantly stronger using GRACE, especially in the northeastern part of the Atlantic Ocean. This will be discussed in section 6.

Table 2 shows the root mean square (RMS) of the gridded residuals trends over 2004-2019, averaged over the Pacific, Indian, North and South Atlantic Oceans for the reanalyses and GRACE cases.

If we exclude FOAM which displays higher RMS in the Indian and South Atlantic oceans than other reanalyses, Table 2 clearly shows systematically higher RMS (in the range 2-3 mm/yr) in the North Atlantic Ocean for the C-GLORS, SODA, GLORYS and ORAS5 reanalyses as well as for GRACE mascons.

Table 2: RMS of gridded residuals trends over 2004-2019, averaged over the Pacific, Indian, North and South Atlantic oceans for the six reanalyses and GRACE mascons cases.

RMS (mm/yr)	Pacific Ocean	Indian Ocean	North Atlantic Ocean	South Atlantic Ocean
C-GLORS	1.48	1.46	2.02	1.35
FOAM	1.66	2.81	1.99	2.54
SODA	1.58	1.79	2.68	1.56
GLORYS	1.34	1.61	2.49	1.72
ORAS5	1.39	1.38	2.15	1.37
CIGAR	1.51	1.51	2.47	1.46
GRACE mascons	1.51	1.78	2.92	1.43

Because four of the reanalyses used above assimilate altimetry data (i.e., C-GLORS, GLORYS, ORAS5 and FOAM), our approach may introduce some circularity to the regional sea level budget assessment. This is the reason for also using reanalyses without altimetry data assimilation (SODA and CIGAR). Here we focus on CIGAR and extend the study period to December 2022. Comparing the manometric components of two reanalyses with and without altimetry data assimilation (e.g., C-GLORS and CIGAR, noting however that they differ in terms of resolution, configuration and forcing ; Figure 4) shows some differences locally, in particular in the northwestern Atlantic and North Indian Oceans. However, the residual trend maps are very similar. ~~In~~ Figure 5 ~~are~~ shows~~n~~ manometric and residual trend maps based on CIGAR, GRACE mascons and GRACE SH ensemble, extended until 2022. Overall, the patterns are qualitatively similar to those of the shorter period 2004-2019 (Figures 3 and 4). Thus, adding three more years does not change the previous conclusion, i.e., that significant residual trends are observed in the North Atlantic (and around Antarctica as well). But the residual patterns in the North Atlantic are noticeably different between CIGAR and GRACE, the maximum signal being located in the western part of the basin for CIGAR and in the eastern part for GRACE.

One may wonder whether the salinity drift observed in some Argo floats as of 2015 has impacted the CIGAR reanalysis since, unlike for altimetry data, T/S data are assimilated during the reanalysis integration, thus non-linearly interacting with dynamical processes. In the reanalysis, the treatment of the salinity drift simply consisted in rejecting data that Argo had flagged for rejection in the delayed mode. But this may not fully guarantee that all bad salinity data have been discarded, possibly leading to a shift in the circulation~~.~~ However, to compute the reanalysis-based manometric component, the local steric contribution has been removed. Thus, any effect of the spurious Argo salinity drift may ~~can~~ be considered as minimal.

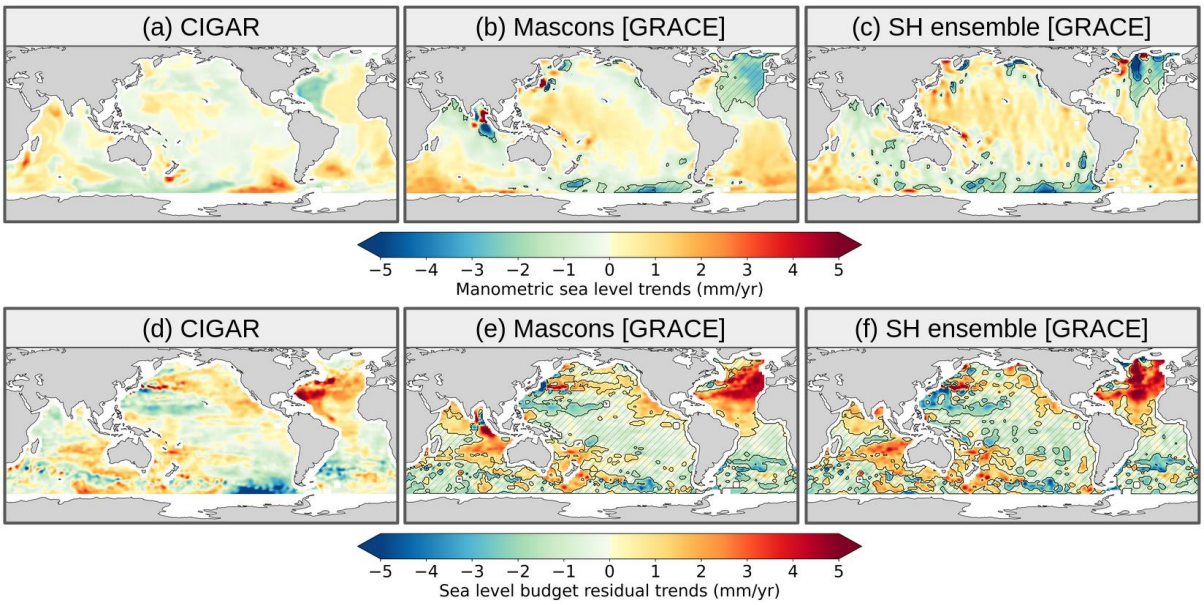

Figure 5: Manometric component based on the CIGAR reanalysis (reanalysis without altimetry data assimilation) (panel a), and the two GRACE solutions (panels b and c). Sea level budget residuals using the CIGAR-based manometric component (panel d) and the two GRACE manometric components (panels e and f). The period of analysis here is from January 2004 to December 2022. Hatched areas in panels (5b,5c, 5e, 5f represent regions where the signal is not significant.

6. Residual trends in the North Atlantic Ocean

In this section, we focus on the North Atlantic Ocean where significant positive residuals are observed when using either GRACE or the CIGAR reanalysis for estimating the manometric component.

Figure 6 shows each component of the budget over the North Atlantic Ocean over January 2004-December 2022, including the three manometric component estimates : GRACE mascons, ensemble mean GRACE SH and CIGAR reanalysis. Associated residual maps (all components unchanged except the manometric one) are also shown.

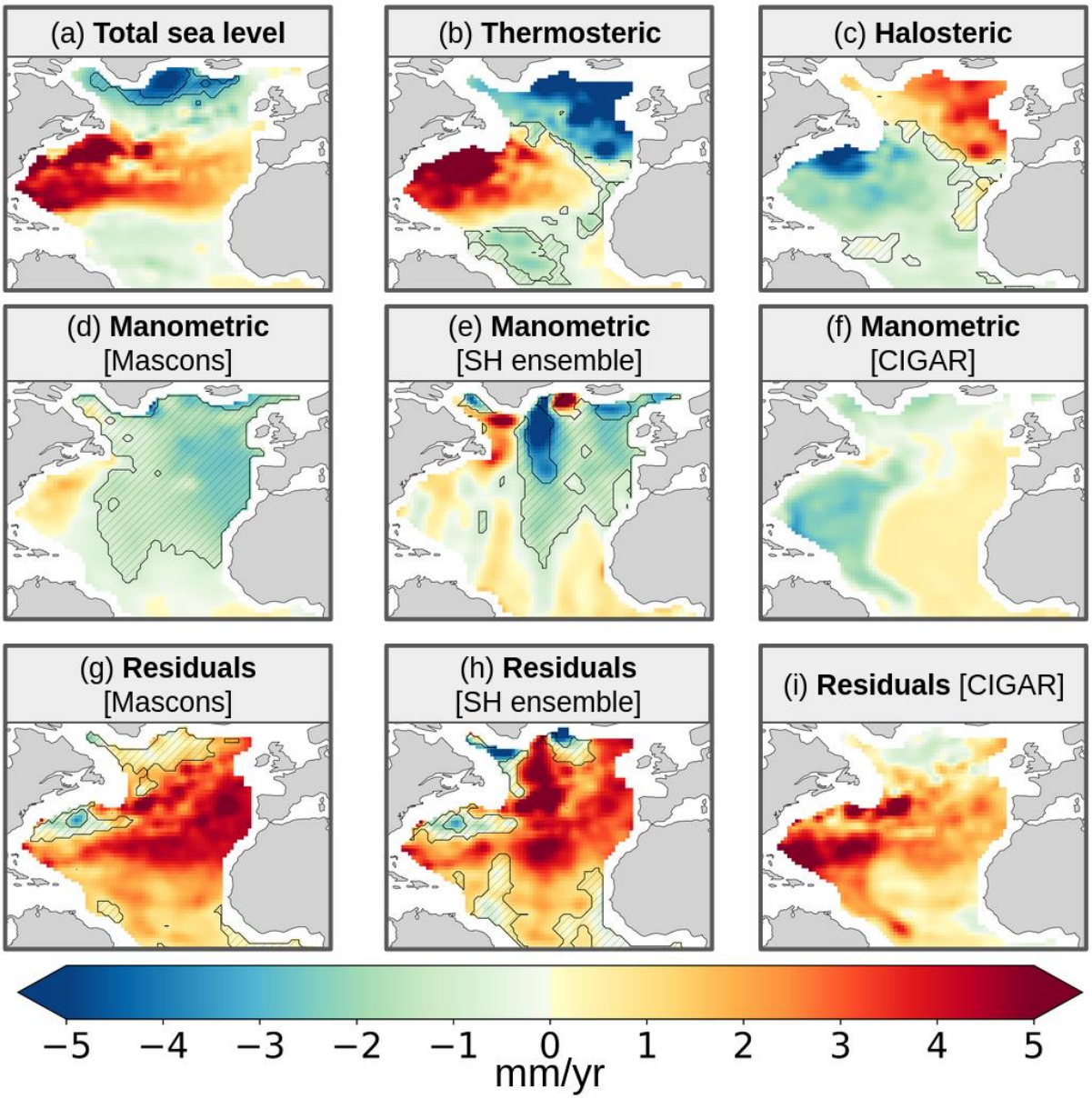

592

593 *Figure 6: North Atlantic Ocean sea level trends (mm/yr) over January 2004 to December 2022:*
594 *Observed altimetry-based sea level (a), Argo-based thermosteric and halosteric components*
595 *(b,c), manometric components from GRACE mascons (d), ensemble mean GRACE spherical*
596 *harmonics (e) and derived from CIGAR reanalysis (f). Sea level budget residuals (observed*
597 *sea level trends minus sum of component trends) using GRACE mascons (g), ensemble mean*
598 *GRACE spherical harmonics (h) and CIGAR (i). Hatched areas represent regions where*
599 *the signal is not significant.*
600

601

602 The North Atlantic Ocean residuals of all three manometric component cases (GRACE
603 mascons, ensemble mean GRACE spherical harmonics and CIGAR) show a positive signal.
604 However, the patterns are significantly different between the reanalysis and GRACE cases.
605 They are localized in the western part of the tropical North Atlantic Ocean with the CIGAR

606 reanalysis and in the eastern part (between the Gibraltar Strait and the Gascogne Gulf) with
607 GRACE mascons. The residuals based on the ensemble mean GRACE spherical harmonics
608 display a strong north-south signal in the mid North Atlantic, likely due to north-south stripe
609 noise affecting spherical harmonic solutions (Blazquez et al., 2018).

610 To further investigate the North Atlantic sea level misclosure, we computed the North Atlantic
611 sea level budget after geographically averaging each component over the region, using
612 GRACE mascons for the manometric component. This is shown in Figure 7 , along with the
613 sea level budget, averaging the data globally but excluding the North Atlantic Ocean.

614

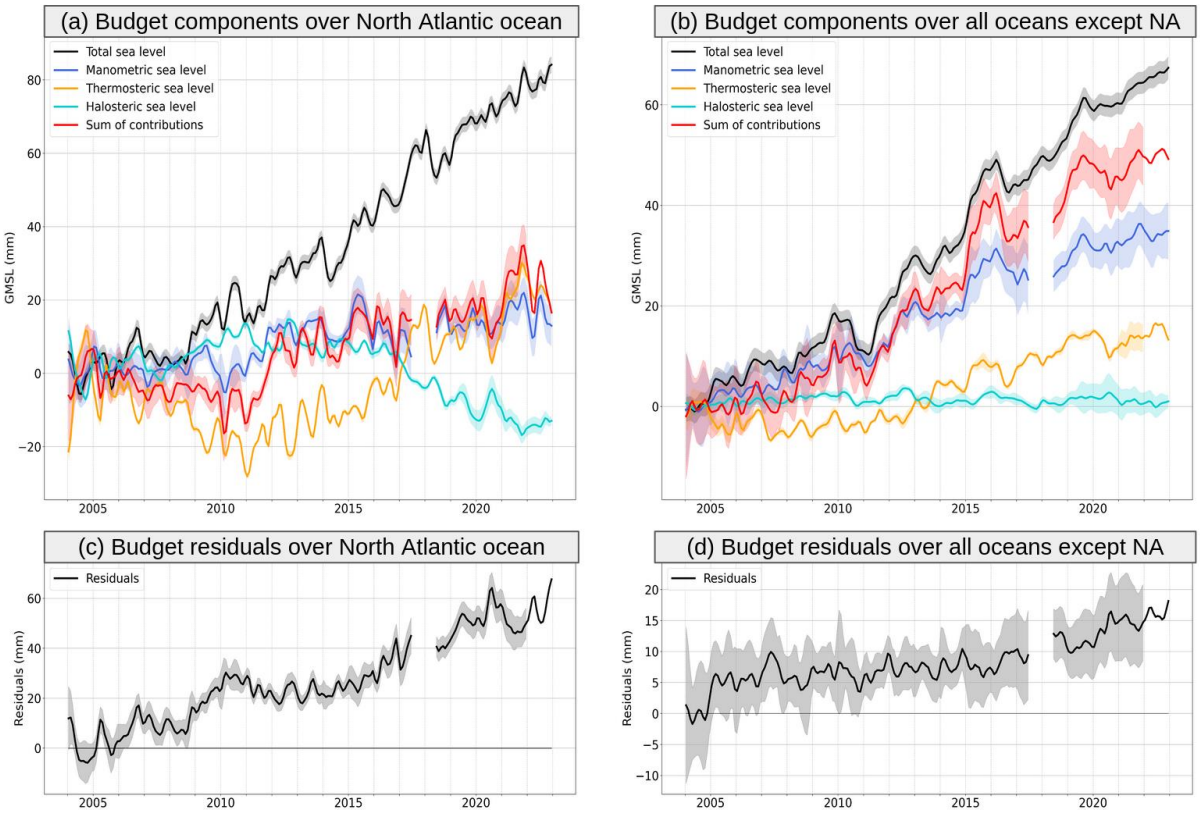

615

616 *Figure 7: Regionally averaged sea level budget for January 2004 to December 2022, over the*
617 *North Atlantic Ocean (a) and over all oceans except the North Atlantic (NA) one (b). On each*
618 *panel are shown the altimetry-based sea level (black curve), the thermosteric and halosteric*
619 *components (orange and turquoise curves), the manometric component (GRACE mascons,*
620 *blue curve) and the sum of all components (red curve). The panels c and d show the*
621 *corresponding residuals (observed sea level minus sum of components). Shaded areas*
622 *represent the standard one-sigma uncertainties.*

623 Figure ,7 well confirms the non-closure of the trend budget over the North Atlantic Ocean.
624 While in Figure 7c the North Atlantic residuals display a positive trend over the whole period
625 (like in Figure 7d), there is a clear shift towards higher residuals around 2015, that may be
626 directly linked to the strongly negative trend as of 2015 of the halosteric component of the

North Atlantic (Figure 7a) ~~with a significant positive residual trend, whereas in the remaining oceanic domain, no significant residual trend is noticed. Figure 7 (panel a) suggests that the North Atlantic residual trend is related to the observed decrease of the halosteric component as of 2015~~. A similar finding is provided in Mu et al. (2024).

In order to check whether the North Atlantic residual signal better fits a trend over the study period rather than a low frequency oscillation, we performed an EOF decomposition over 2004-2022 of the gridded residual time series (considering the GRACE SH solution for the manometric component) (see Figure S3 in the Supplementary Information, showing the first two EOF modes). Mode 1 is dominated by a strong residual trend in the North Atlantic. Its spatial map is very similar to the residual map. Mode 2 shows an oscillation of period ~11 years on which are superimposed shorter fluctuations related to ENSO. This EOF decomposition of the residuals confirms the dominant trend contribution of the North Atlantic over the study period.

7. Conclusion

In this study, we have revisited the regional sea level trend budget over the GRACE and Argo era. Using different data sets for the manometric component (GRACE and ocean reanalyses), we found significant non-closure of the trend budget in the North Atlantic Ocean in all studied cases. However, the residual patterns are not localized over the same areas in the GRACE and ocean reanalyses cases. They are stronger in the northeast Atlantic Ocean when considering the GRACE manometric component (mascon solution) while they are more localized in the northwestern tropical part with the reanalysis-based manometric component. The sea level budget averaged over the whole North Atlantic Ocean leads us to suspect the steric contribution, especially the halosteric component as the main contributor to the budget non-closure in this region, considering that the global budget without the North Atlantic region is closed within the error bars. Although we chose the SIO data set to estimate the steric component, considering that the salinity data had been corrected for the Argo floats instrumental drift that led to spurious salinity measurements, our study points to remaining errors affecting the halosteric component, especially as of 2015. Mu et al. (2024) also report a potential salinity bias in the Argo data set of the North Atlantic. Our results suggest that the salinity adjustment to the WOCE salinity climatology proposed by the SIO methodology may not fully correct for the rapid salinity drift experienced by some Argo floats. However, the

different locations of the North Atlantic residual patterns when considering the reanalyses or GRACE for the manometric component, as well as larger residuals in the northeast Atlantic Ocean in the GRACE case, suggest that uncertainty in GRACE data also plays a role. In other oceanic regions, a few areas display small-scale residual structures (e.g., in the north and eastern Pacific and northwest Indian Ocean). This may eventually result from differences in resolution of the gridded data sets used in this study (e.g., satellite altimetry better resolves small scale features than GRACE or Argo), even though the same low pass filter was applied to all data sets.

The problem of the North Atlantic halosteric component highlighted in our regional trend budget study needs to be fixed up at the processing level of the Argo-based measurements. Our findings are helpful to the scientific groups involved in the Argo network as we can identify regions where the salinity contribution to regional sea level change appears to be spurious. This may help them in refining their investigations on the quality control checks to be applied to the Argo profiles. In addition, detailed investigation of the GRACE contribution to the residuals of this region should also be carried out in parallel. Our study highlights the necessity of applying consistent data processing and using similar reference systems for satellite altimetry and gravimetry data. Improved data should indeed be made available to the community, not only for sea level budget assessments but also for other applications in oceanography or climate-related research (i.e., for Earth's energy imbalance studies based on sea level budget approaches).

Acknowledgements

We thank two anonymous reviewers for their helpful comments. We also thank the Magellium/LEGOS climate change team for providing us with the ensemble mean of the GRACE-based spherical harmonics solutions and fruitful discussions.

This research was carried out under a programme of, and funded by, the European Space Agency (ESA) Climate Change Initiative, within the project entitled "Sea level budget closure CCI+ (SLBC_CCI+)" (contract number 4000140620/23/I-BN). Part of this work is a contribution to the GREAT project which is supported by the Centre National d'Etudes Spatiales (CNES) through the Ocean Surface Topography Science Team (OSTST). Part of this work was also performed in the context of the ERC Synergy GRACEFUL project (ERC Synergy grant n° 855677).

Authors contribution

Conceptualization: MB, AB (Barnoud), AC; Data analysis: MB, AB (Barnoud); Reanalysis computation: CY, AS: Writing of the original draft: AC; Final writing, review and editing: all co-authors.

Conflict of interest

The authors declare no conflict of interest relevant to this study.

References

Ablain M., R. Jugier, L. Zawadki, and N. Taburet (2017). "The TOPEX-A Drift and Impacts on GMSL Time Series." AVISO Website. October 2017. https://meetings.aviso.altimetry.fr/fileadmin/user_upload/tx_ausyclsseminar/files/Poster_OSTST17_GMSL_Drift_TOPEX-A.pdf.

Ablain, M., Meyssignac B., Zawadski, L., Jugler R., Ribes, A., Spada, G., Benveniste, J., Cazenave, A. and Picot, N. (2019), Uncertainty in satellite estimates of global mean sea-level changes, trend and acceleration, *Earth Syst. Sci. Data*, 11, 1189–1202.

Adhikari, S., Ivins, E. R., Frederikse, T., Landerer, F. W., and Caron, L. (2019). Sea-level fingerprints emergent from GRACE mission data, *Earth Syst. Sci. Data*, 11, 629–646, https://doi.org/10.5194/essd-11-629-2019.

Barnoud, A., Pfeffer, J., Cazenave, A., Fraudeau, R., Rousseau, V., & Ablain, M. (2023). Revisiting the global mean ocean mass budget over 2005–2020. *Ocean Science*, 19, 321–334, https://doi.org/10.5194/os-19-321-2023.

Barnoud A. et al. (2021). Contributions of altimetry and Argo to non-closure of the global mean sea level budget since 2016, published online 26 June 2021, *Geophys. Res. Lett.*, https://doi.org/10.1029/2021GL092824.

Blazquez A., Meyssignac B., Lemoine J.M., Berthier E., Ribes A. and Cazenave A. (2018). Exploring the uncertainty in GRACE estimates of the mass redistributions at the Earth' surface. Implications for the global water and sea level budgets, *Geophysical Journal International*, 215(1), 415-430.

Blockley, E. W., Martin, M. J., McLaren, A. J., Ryan, A. G., Waters, J., Lea, D. J., Mirouze, I., Peterson, K. A., Sellar, A., and Storkey, D. (2014). Recent development of the Met Office operational ocean forecasting system: an overview and assessment of the new Global FOAM forecasts, *Geosci. Model Dev.*, 7, 2613–2638, https://doi.org/10.5194/gmd-7-2613-2014.

Brown S, Willis J, Fournier S. (2023). Jason-3 wet path delay correction. Ver. F. PO.DAAC, CA, USA. https://doi.org/10.5067/J3L2G-PDCOR.

729 Camargo C.M. et al. (2023). Regionalizing the sea level budget with machine learning
730 techniques, *Ocean Science*, 19, 17-41, https://doi.org/10.5194/os-19-17-2023.

731 Caron, L., Ivins, E. R., Larour, E., Adhikari, S., Nilsson, J., & Blewitt, G. (2018). GIA model
732 statistics for GRACE hydrology, cryosphere and ocean science. *Geophysical Research*
733 *Letters*, 45, 2203– 2212. https://doi.org/10.1002/2017GL07664.

734 Carrere L. and Lyard F. (2003), Modeling the barotropic response of the global ocean to
735 atmospheric wind and pressure forcing. Comparisons with observations. *Geophys. Res. Lett.*
736 30, 6, 1275, https://doi.org/10.1029/2002GL016473.

737 Carret, A., Llovel, W., Penduff, T., & Molines, J.-M. (2021). Atmospherically forced and chaotic
738 interannual variability of regional sea level and its components over 1993–2015. *Journal of*
739 *Geophysical Research: Oceans*, 126, e2020JC017123.
740 https://doi.org/10.1029/2020JC017123

741 Carret A., Johannessen J., Andersen O., Ablain M., Prandi P., Blazquez A. and Cazenave A.
742 (2017). Arctic sea level during the altimetry era, *Surveys in Geophysics*, 38, 251-277,
743 https://doi.org/10.1007/s10712-016-9390-2.

744 Carton, J. A., G. A. Chepurin, and L. Chen (2018). SODA3: A New Ocean Climate Reanalysis.
745 *J. Climate*, 31, 6967–6983, https://doi.org/10.1175/JCLI-D-18-0149.1.

746 Cazenave A., Palanisamy H. and Ablain M. (2018). Contemporary sea level changes from
747 satellite altimetry: What have we learned? What are the new challenges? *Advances in Space*
748 *Research*, https://doi.org/10.1016/j.asr.2018.07.017, published online 27 July 2018.

749 Cazenave A. and Moreira L. (2022). Contemporary sea level changes from global to local
750 scales: a review, *Proc. Royal Society*, 478, 20220049.
751 https://doi.org/10.1098/rspa.2022.0049.

752 Chen, J.L., Tapley, B. D., Save, H., Tamisiea, M. E., Bettadpur, S., & Ries, J. (2018). Quantification
753 of ocean mass change using gravity recovery and climate experiment, satellite altimeter, and Argo
754 floats observations. *Journal of Geophysical Research: Solid Earth*, 123, 10,212–10,225.
755 https://doi.org/10.1029/2018JB016095.

756

757 Chen J.L., Tapley B.D., Seo K-W., Wilson C. and Ries J. (2019), Improved Quantification of
758 Global Mean Ocean Mass Change Using GRACE Satellite Gravimetry Measurements ».
759 *Geophysical Research Letters* 46, 23, 13984-91. https://doi.org/10.1029/2019GL085519.

760 Chen J.L., Tapley B.D., Wilson C., Cazenave A., Seo K-W. and Kim J.S. (2020). Global ocean
761 mass change from GRACE 1 and GRACE Follow-On, and altimeter and Argo measurements,
762 *Geophys. Res. Lett*., https://doi.org/10.1029/2020GL090656, published online, 3 November
763 2020.

764 Dangendorf S, Frederikse T, Chafik L, Klinck JM, Ezer T, Hamlington BD. (2021). Data-driven
765 reconstruction reveals large-scale ocean circulation control on coastal sea level. *Nat.*
766 *Clim.Change* 11, 514–520. https://doi.org/10.1038/s41558-021-01046-1.

767 Dieng H.B., Cazenave A., Meyssignac B. and Ablain M. (2017). New estimate of the current
768 rate of sea level rise from a sea level budget approach, *Geophys. Res. Lett*., 44,
769 https://doi/org/10.1002/2017GL073308.

Dobslaw, H., Bergmann-Wolf, I., Dill, R., Poropat, L., Thomas, M., Dahle, C., et al. (2017). A new high-resolution model of non-tidal atmosphere and ocean mass variability for de-aliasing of satellite gravity observations: AOD1B RL06. *Geophysical Journal International*, 211(1), 263-269, https://doi.org/10.1093/gji/ggx302.

England, M.H., McGregor, S., Spence, P., Meehl, G. A. (2014). Recent intensification of wind-driven circulation in the Pacific and the ongoing warming hiatus. *Nature Climate Change*, **4**, 222-227, https://doi.org/10.1038/NCLIMATE2106.

Flechtner, F., Dobslaw, H. & Fagiolini, E. (2015). AOD1B Product Descrip tion Document for Product Release 05 Rev4.4 GRACE 327–750, Geo Forschungszentrum Potsdam, Potsdam, Germany.

Forget, G., and Ponte, R. M. (2015). The partition of regional sea level variability. *Progr. Oceanogr*. 137, 173–195. https://doi.org/10.1016/j.pocean.2015.06.002.

Frederikse, T., Riva, R., Kleinherenbrink, M., Wada, Y., den Broeke, M. van, and Marzeion, B. (2016), Closing the sea level budget on a regional scale: Trends and variability on the Northwestern European continental shelf, *Geophys. Res. Lett*., 43, 10,864– 10,872, https://doi.org/10.1002/2016GL070750.

Frederikse, T., Jevrejeva, S., Riva, R. E. M., & Dangendorf, S. (2018). A Consistent Sea-Level Reconstruction and Its Budget on Basin and Global Scales over 1958–2014, *Journal of Climate*, 31(3), 1267-1280, https://journals.ametsoc.org/view/journals/clim/31/3/jcli-d-17-0502.1.xml.

Frederikse T et al. (2020). The causes of sea-level rise since 1900. *Nature* 584, 393–397, https://doi.org/10.1038/s41586-020-2591-3.

Garric, G., and Parent, L. (2017). Quality Information Document for Global 1330 Ocean Reanalysis Products Global-Reanalysis-Phy-001-025. Available online at: https://catalogue.marine.copernicus.eu/documents/QUID/CMEMS-GLO-QUID-001-025.pdf

Gregory, J. M. & Lowe, J. A. (2000). Predictions of global and regional sea-level rise using AOGCMs with and without flux adjustment. *Geophysical Research Letters*, 27(19), 3069-3072. https://doi.org/10.1029/1999GL011228.

Gregory J.M. et al. (2019). Concepts and Terminology for Sea Level: Mean, Variability and Change, Both Local and Global, *Surveys in Geophysics*, 40:1251–1289, https://doi.org/10.1007/s10712-019-09525-z.

Good, S. A., M. J. Martin and N. A. Rayner (2013). EN4: quality controlled ocean temperature and salinity profiles and monthly objective analyses with uncertainty estimates, *Journal of Geophysical Research: Oceans*, 118, 6704-6716, https://doi;org/10.1002/2013JC009067.

Guérou, A., Meyssignac, B., Prandi, P., Ablain, M., Ribes, A., and Bignalet-Cazalet, F. (2023). Current observed global mean sea level rise and acceleration estimated from satellite altimetry and the associated measurement uncertainty, *Ocean Sci.,* 19, 431–451, https://doi.org/10.5194/os-19-431-2023.

Hamlington et al. (2020). Under standing contemporary regional sea level change and the implications for the future, *Review of Geophysics*, https://doi.org/10.1029/2019RG000672.

Hamlington, B. D., Cheon, S. H., Piecuch, C. G., Karnauskas, K. B., Thompson, P. R., Kim, K.-Y., et al. (2019). The dominant global modes of recent internal sea level variability. *Journal of Geophysical Research: Oceans*, 124, 2750–2768. https://doi.org/10.1029/2018JC014635.

Han, W., Meehl, G., Stammer, D., Hu, A., Hamlington, B., Kenigson, J., et al. (2017). Spatial patterns of sea level variability associated with natural internal climate modes. *Surveys in Geophysics*, 38(1), 217–250. https://doi.org/10.1007/s10712-016-9386-y.

Han W., Stammer D., Thompson P., Ezer T., Palanisamy H., Zhang X., Domingues C., Zhang L., Yuan D., (2019). Impacts of Basin-Scale Climate Modes on Coastal Sea Level: a Review, *Surveys in Geophysics*, 40, 1493–1541, https://doi.org/10.1007/s10712-019-09562-8.

Horwath M., Gutknetch B., Cazenave A., et al., (2022). Global sea level budget and ocean mass budget, with focus on advanced data products and uncertainty characterization. *Earth System Science Data*, 14, 411–447, 2022 https://doi.org/10.5194/essd-14-411-2022.

IPCC (2019). IPCC Special Report on the Ocean and Cryosphere in a Changing Climate, edited by Portner, H.-O., Roberts, D. C., Masson-Delmotte, V., Zhai, P., Tignor, M., Poloczanska, E., Mintenbeck, K., Alegriìa, A., Nicolai, M., Okem, A., Petzold, J., Rama, B., and Weyer, N. M.

IPCC (2021), Climate Change 2021. The Physical Science Basis. Contribution of Working Group I to the Sixth Assessment Report of the Intergovernmental Panel on Climate Change [Masson-Delmotte, V., P. Zhai, A. Pirani, S.L. Connors, C. Péan, S. Berger, N. Caud, Y. Chen, L. Goldfarb, M.I. Gomis, M. Huang, K. Leitzell, E. Lonnoy, J.B.R. Matthews, T.K. Maycock, T. Waterfield, O. Yelekçi, R. Yu, and B. Zhou (eds.)]. Cambridge University Press. In Press.

Llovel, W., and T. Lee (2015), Importance and origin of halosteric contribution to sea level change in the southeast Indian Ocean during 2005–2013, *Geophys. Res. Lett.*, 42, 1148–1157, https://doi.org/10.1002/2014GL062611.

Llovel, W., Balem, K., Tajouri, S., & Hochet, A. (2023). Cause of substantial global mean sea level rise over 2014–2016. *Geophysical Research Letters*, 50, e2023GL104709. https://doi.org/10.1029/2023GL104709.

Loomis, B. D., Luthcke, S. B., & Sabaka, T. J. (2019). Regularization and error characterization of GRACE mascons. *Journal of Geodesy*, 93(9), 1381–1398. https://doi.org/10.1007/s00190-019-01252-y.

Lorbacher, K., Marsland, S. J., Church, J. A., Griffies, S. M., Stammer, D. (2012). Rapid barotropic sea level rise from ice sheet melting. *Journal of Geophysical Research*, 117, C06003, https://doi.org/10.1029/2011JC007733.

Liu C., Liang X., Ponte R.M.. and Chambers D.P. (2020). Global patterns of spatial and temporal variability in multiple gridded salinity products, *J. Climate*, 33, 20, 8751-8766, https://doi.org/10.1175/jcli-d-20-0053.1.

Liu C., Liang X., Ponte R.M. and Chambers D.P. (2024). 3Salty Drifts" of argo floats affects the gridded ocean salinity products, *J. Geophys. Res. -Oceans*, 129, c2023JC020871, https://doi.org/10.1019/2023JC020871.

Ludwigsen C.B. et al. (2024). Global and regional ocean mass budget closure since 2003, *Nature Communications,* 15, 1416, https://doi.org/10.1038/s41467-024-45726-w.

851 Ludwigsen C.B., Andersen O.B. and rose S.K. (2022), Components of 20 years (1995-2015)
852 of absolute sea level trends in the Arctic, *Ocean Science*, 181,109-127,
853 https://doi.org/10.5194/os-18-109-2022.

854 Merrifield, M. A., and Maltrud, M. E. (2011), Regional sea level trends due to a Pacific trade
855 wind intensification, *Geophys. Res. Lett.*, 38, L21605, https://doi.org/10.1029/2011GL049576.

856 Milne G.A., Gehrels W.R., Hughes C.W. and Tamisea M.E. (2009), Identifying the causes of
857 sea level change, *Nature Geosci* 2, 471–478. https://doi.org/10.1038/ngeo544.

858 Mitrovica J, Tamisiea ME, Davis JL, Milne GA. (2001). Recent mass balance of polar ice
859 sheets inferred from patterns of global sea-level change. *Nature,* 409, 1026–1029,
860 https://doi.org/10.1038/35059054.

861 Mu D., Church J.A., King M., Ludwigsen C.B. and Xu T. (2024). Contrasting discrepancy in
862 the sea level budget between the North and South Atlantic Ocean since 2016, *Earth and*
863 *Space Science,* 11, e2023EA003133, https://doi.org/10.1029/2023EA003133.

864 Nerem, R.S., Beckley, B.D., Fasullo, J., Hamlington, B.D., Masters, D. and Mitchum, G.T.
865 (2018). Climate Change Driven Accelerated Sea Level Rise Detected In The Altimeter Era,
866 *Proceedings of the National Academy of Sciences,* 15, 9, 2022-2025,
867 https://doi.org/10.1073/pnas.1717312115.

868 Peltier R.W. (2004), Global Glacial Isostasy and the Surface of the Ice-Age Earth: The ICE-
869 5G (VM2) Model and GRACE, *Annual Review of Earth and Planetary Science*, 32, 111-149.

870 Peltier R.W., D. F. Argus, and R. Drummond (2018). "Comment on “An assessment of the
871 ICE-6G_C (VM5a) glacial isostatic adjustment model” by Purcell et al." *Journal of Geophysical*
872 *Research- Solid Earth* 123, 2, 2019-2028.

873 Piecuch CG and Ponte RM. (2014). Mechanisms of global mean steric sea level change. *J.*
874 *Clim.* 27, 824–834, https://doi.org/10.1175/JCLI-D-13-00373.1.

875 Ponte R.M., Sun Q., Liu C. and Liang X. (2021). How salty is the global ocean: weighting it all
876 or tasting it a sip at a time, *Geophys. Res. Lett.*, 48, 11, e2021GL092935,
877 https://doi.org/10.1029/2021gl092935.

878 Prandi, P., Meyssignac, B., Ablain, M. et al. (2021). Local sea level trends, accelerations and
879 uncertainties over 1993–2019*. Nature Sci Data*, 626, 8, 1. https://doi.org/10.1038/s41597-020-
880 00786-7.

881 Proshutinsky AIM, Ashik EN, Dvorkin S, Häkkinen RA, Krishfield PWR. (2004). Secular sea
882 level change in the Russian sector of the Arctic Ocean. *J. Geophys. Res*. 109, C03042,
883 https://doi.org/10.1029/2003JC002007.

884 Purkey SG, Johnson GC. (2010). Warming of Global Abyssal and Deep Southern Ocean
885 Waters between the 1990 s and 2000 s, contributions to Global Heat and Sea Level Rise
886 Budgets. *J. Clim.* 23, 6336–6351, https://doi.org/10.1175/2010JCLI3682.1.

887 Rietbroek, R., Brunnabend, S. E., Kusche, J., Schröter, J., and Dahle, C. (2016). Revisiting
888 the contemporary sea-level budget on global and regional scales. *Proc. Natl. Acad. Sci.*, 113,
889 1504–1509. https://doi.org/10.1073/pnas.1519132113.

Roberts CD, Calvert D, Dunstone N, Hermanson L, Palmer MD, Smith D. (2016). On the drivers and predictability of seasonal to interannual variations in regional sea level. J. Clim. 29, 7565–7583, https://doi.org/10.1175/JCLID-D-15-0886.1.

Roemmich D, Gilson J. (2009). The 2004–2008 mean and annual cycle of temperature, salinity, and steric height in the global ocean from the Argo Program. *Prog. Oceanogr.* 82, 81–100, https://doi.org/10.1016/j.pocean.2009.03.004.

Royston, S., Vishwakarma, B. D., Westaway, R. M., Rougier, J., Sha, Z., and Bamber, J. L. (2020). Can we resolve the basin-scale sea level trend budget from GRACE ocean mass? *Journal of Geophysical Research- Oceans*, 125, e2019JC015535. 558, https://doi.org/10.1029/2019JC015535.

Save H., Bettadpur S. and Tapley B.D. (2016). High resolution CSR GRACE RL05 mascons, *J. Geophys. Res. Solid Earth*, 121, 7547-7569, https://doi.org/10.1002/2016jB013007.

Spada, G. (2017). Glacial isostatic adjustment and contemporary sea level rise: An overview. *Surveys in Geophysics*, 38, 153- 587 185. https://doi.org/10.1007/s10712-016-9379-x.

Sun, Y., Riva, R., & Ditmar, P. (2016). Optimizing estimates of annual variations and trends in geocenter motion and J2 from a combination of GRACE data and geophysical models. *Journal of Geophysical Research,* 121(11), 8352-8370. https://doi.org/10.1002/2016JB013073.

Stammer D., Cazenave A., Ponte R. M., Tamisiea M. E. (2013). Causes for contemporary regional sea level changes. *Ann Rev Mar Sci.* 567, 5, 21- 46. https://doi.org/10.1146/annurev-marine-121211-172406.

Storto, A. and Masina, S (2016). C-GLORSv5: an improved multipurpose global ocean eddy-permitting physical reanalysis, *Earth Syst. Sci. Data*, 8, 679–696, https://doi.org/10.5194/essd-8-679-2016.

Storto, A., Yang, C. (2024). Acceleration of the ocean warming from 1961 to 2022 unveiled by large-ensemble reanalyses. *Nat Commun* 15, 54, https://doi.org/10.1038/s41467-024-44749-7.

Storto, A., Chierici, G., Pfeffer, J., Barnoud, A., Bourdalle-Badie, R., Blazquez, A., Cavaliere, D., Lalau, N., Coupry, B., Drevillon, M., Fourest, S., Larnicol, G., and Yang, C. (2024). Variability in manometric sea level from reanalyses and observation-based products over the Arctic and North Atlantic oceans and the Mediterranean Sea, in: 8th edition of the Copernicus Ocean State Report (OSR8), edited by: von Schuckmann, K., Moreira, L., Grégoire, M., Marcos, M., Staneva, J., Brasseur, P., Garric, G., Lionello, P., Karstensen, J., and Neukermans, G., Copernicus Publications, State Planet, 4-osr8, 12, https://doi.org/10.5194/sp-4-osr8-12-2024.

Swenson, S., Chambers, D., & Wahr, J. (2008). Estimating geocenter variations from a combination of GRACE and ocean model output. *Journal of Geophysical Research*, 113, B8410. https://doi.org/10.1029/2007JB005338.

Tamisiea, M. E. (2011). Ongoing glacial isostatic contributions to observations of sea level change. *Geophys. J. Int*. 186, 1036–1044. https://doi.org/10.1111/j.1365-246X.2011.05116.x.

Tajouri S., W. Llovel, F. Sévellec, J.M. Molines, P. Mathiot, et al. (2024). Simulated Impact of Time-Varying River Runoff and Greenland Freshwater Discharge on Sea Level Variability in the Beaufort Gyre Over 2005–2018. *Journal of Geophysical Research. Oceans*, 129, 9, https://doi.org/10.1029/2024JC021237.

933 Tapley, B., Watkins, M. M., Flechtner, F., Reigber, C. et al. (2019). Contributions of GRACE
934 to understanding climate change, *Nature Climate Change*, 9, 358–369.
935 https://doi.org/10.1038/s41558-019-0456-2.

936 Timmermann, A., McGregor, S., Jin, F. -F. (2010), Wind effects on past and future regional
937 sea level trends in the southern Indo-Pacific. *Journal of Clim*ate, **23**(16), 4429–4437,
938 https://doi.org/10.1175/2010JCLI3519.1.

939 Wang O., Lee T., Piecuch C.G., Fukumori I., Fenty I., Frederiske T. et al. (2022). Local and
940 remote forcing of interannual sea level variability at Nantucket Island, *J. Geophys. Res.*
941 *Oceans*, 127, 6,e2021JC018275, https://doi.org/10.1029/2021jc018275.

942 Watkins, M. M., Wiese, D. N., Yuan, D.-N., Boening, C., & Landerer, F. W. (2015). Improved
943 methods for observing Earth's time variable mass distribution with GRACE using spherical cap
944 mascons. *Journal of Geophysical Research: Solid Earth,* 120, 2648–2671.
945 https://doi.org/10.1002/2014JB011547.

946 WCRP Global Sea Level Budget Group (The) (2018). Global sea level budget, 1993-present,
947 *Earth System Science Data*, 10, 1551-1590, https://doi.org/10.5194/essd-10-1551-2018.

948 Wong A., Gilson J. and Cabanes C. (2023). Argo salinity: bias and uncertainty evaluation,
949 *Earth Syst. Sci.data*, 15, 383-393, https://doi.org/10.5194/essd-15-383-2023.

950 Wunsch C and Stammer D. (1997). Atmospheric loading and the oceanic 'inverted barometer'
951 effect. *Rev. Geophys*. 35, 79–107, https://doi.org/10.1029/96RG03037.

952 Zuo H., Balmaseda M.A., Tietsche S., Mogensen K., Mayer M. (2019), The ECMWF
953 operational ensemble reanalysis–analysis system for ocean and sea ice: A description of the
954 system and assessment. *Ocean Sci.* 15, 779–808.

955

956

Supplementary Information

I. Trends and trend uncertainties of altimetry-based total sea level, components and budget residuals over 2004-2022

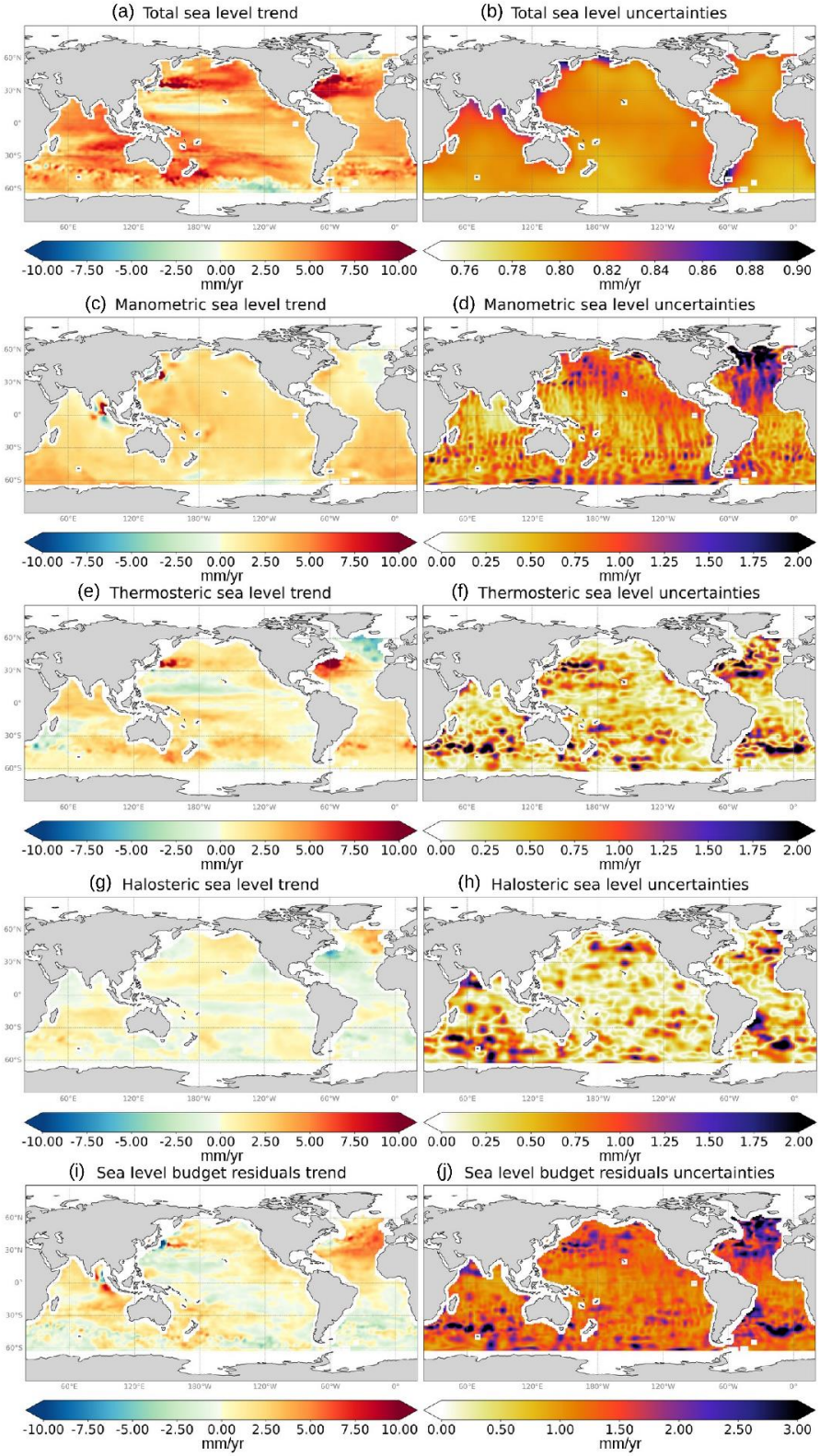

Figure S1: Trend map (left panels) and associated 1-sigma trend uncertainty map (right panels) over 2004-2022 for each term of the regional sea level budget: (a,b) Total altimetry-based sea level trends and associated trend uncertainties, (c,d) GRACE-based manometric component and associated trend uncertainties, (e,f) thermosteric component and associated trend uncertainties, (g,h) halosteric component and associated trend uncertainties, and (i,j) budget residuals and associated trend uncertainties.

II. Sea level budget residuals of the low degree harmonics of the components

In order to highlight the contribution of the different low degree harmonics in the sea level budget residuals, we decomposed each of the components, restricted to their common oceanic mask, in spherical harmonics and computed the sea level budget for different combinations of these low degree harmonics. The sum of all components summed up to degree 4 (Figure S2, top left panel) well reproduces the sea level budget residual map characteristics with high residuals in the North Atlantic Ocean. Other panels of Figure S2 show the residuals of the sea level budget with components summed up to degree 4, with one harmonic signal corresponding to one (degree l, order m) combination. Table S1 provides the root mean squares (RMS) for each case, computed over all oceans. Figure S2 and Table S1 show that residuals are strongly reduced in the North Atlantic Ocean when removing harmonics l1m0 (geocenter term), l1m1, l2m1 (including the polar motion term), l3m2, l3m3 and l4m2. This means that these harmonics contain spurious signals in some of the sea level budget components. Globally and in the North Atlantic Ocean, harmonics l1m0, l2m1 and l4m3 have the highest impact on the residuals.

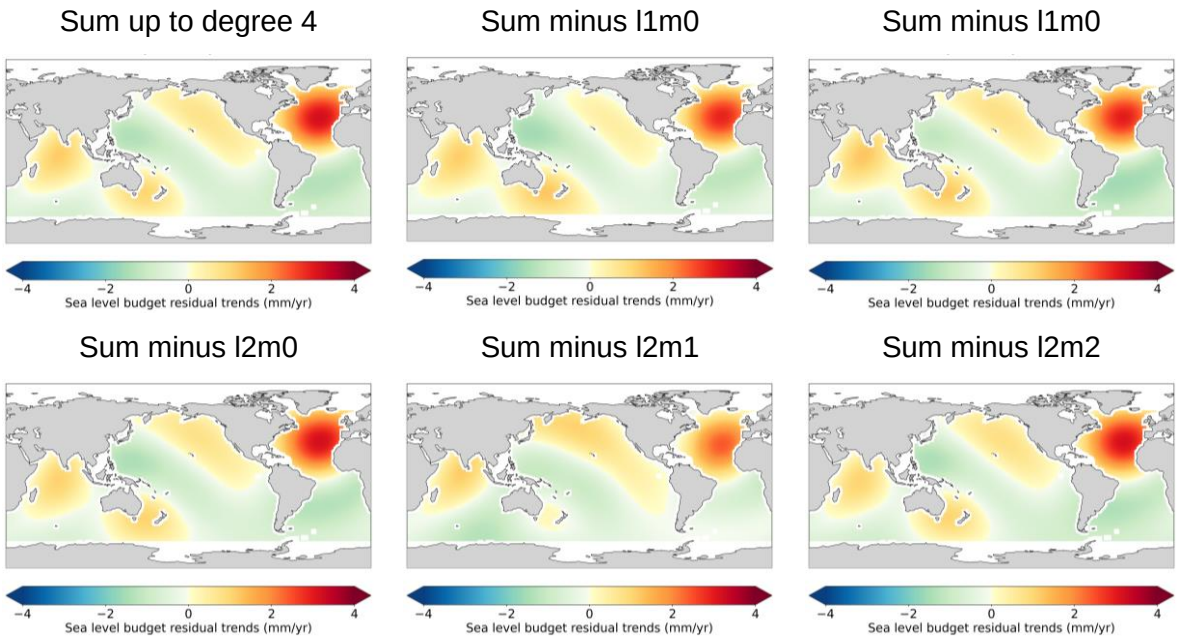

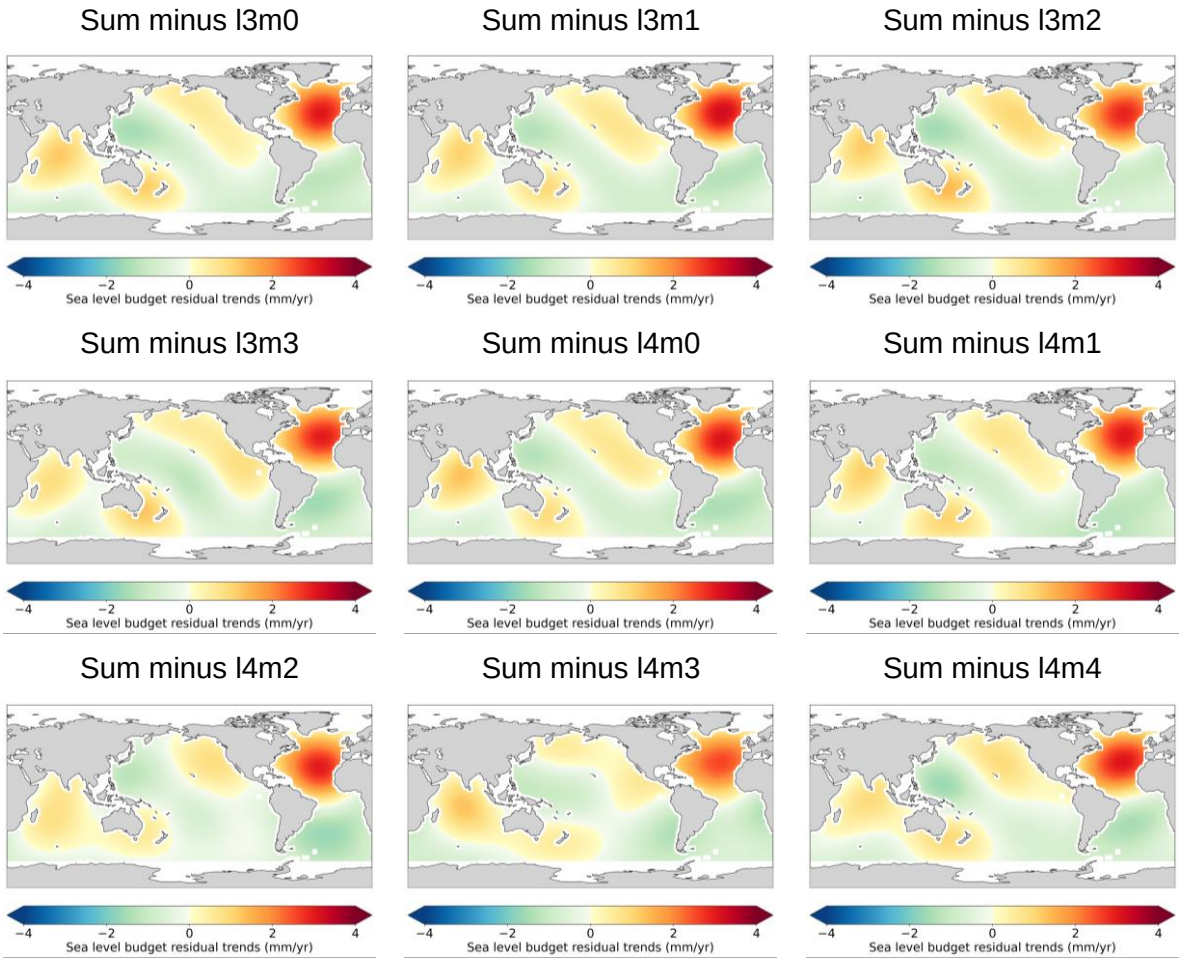

Figure S2: Sea level budget residual trends computed over January 2005 to June 2022 using the low degrees of each component up to degree 4, and subtracting each order/degree contribution one by one.

Table S1: Root mean square (RMS) of the residual trends computed using the low degrees of each component up to degree 4, and subtracting each order/degree contribution one by one. The RMS is computed over the global oceans and over the North Atlantic, South Atlantic, Indian and Pacific Oceans. Bold font indicates RMS values which are lower than 0.1 mm/yr below the value for the sum up to degree 4 without any subtraction (first line).

Component removed from the sum of all components up to degree 4	Residual trends RMS over oceans (mm/yr)				
	Global	North Atlantic	South Atlantic	Indian	Pacific
None	0.94	2.11	1.00	0.55	0.64
l1m0	0.87	**1.86**	**0.87**	0.54	0.65
l1m1	0.92	**1.91**	1.18	0.60	0.60
l2m0	0.94	2.11	0.99	0.51	0.65
l2m1	**0.74**	**1.50**	**0.48**	0.69	0.56

l2m2	0.93	2.08	0.96	0.51	0.64
l3m0	0.92	2.01	0.92	0.59	0.64
l3m1	0.93	2.13	0.98	0.50	0.61
l3m2	0.93	**1.93**	**0.76**	0.58	0.76
l3m3	0.90	**1.95**	1.04	0.46	0.63
l4m0	0.94	2.08	1.04	0.61	0.62
l4m1	0.91	2.03	0.97	0.52	0.61
l4m2	0.90	2.03	1.16	**0.43**	**0.52**
l4m3	0.84	**1.80**	**0.80**	0.64	0.57
l4m4	0.93	2.07	1.03	0.47	0.65

III. EOF Decomposition of the gridded residual time series (with the GRACE SH-based manometric component)

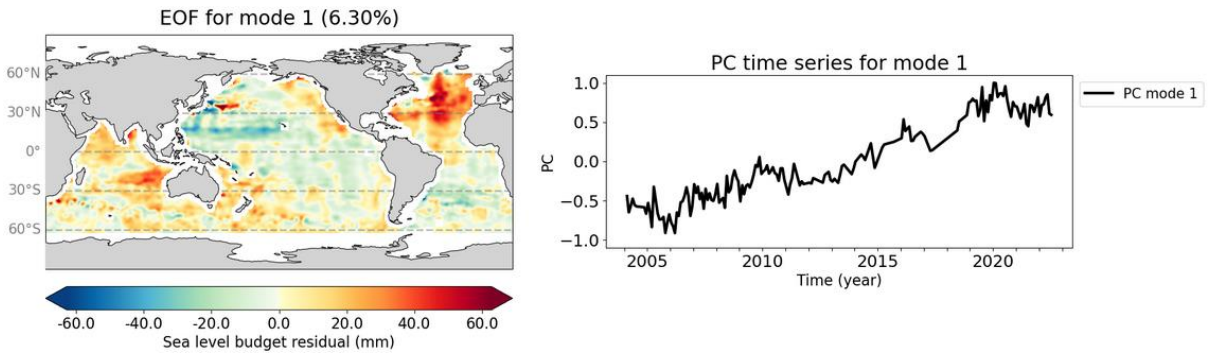

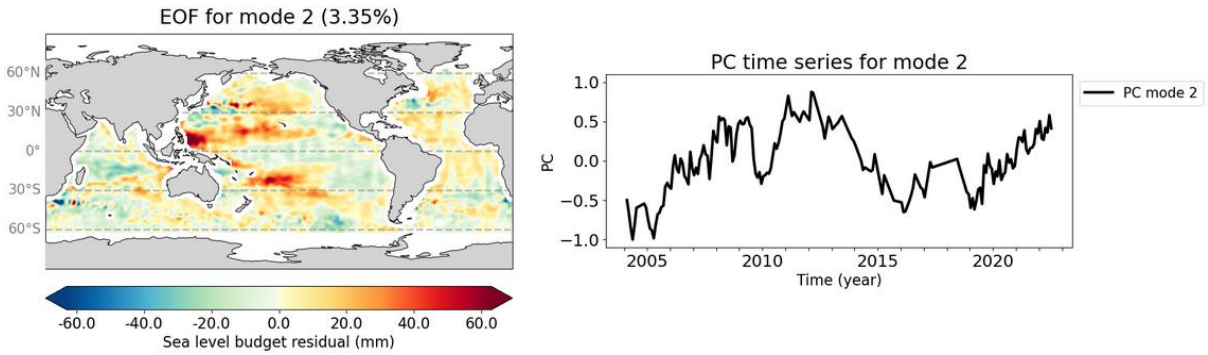

Figure S3: Modes 1 and 2 of the EOF decomposition over 2004-2022 of the gridded residual time series (with the GRACE SH manometric component). The left panels are the spatial maps while the right panels are the associated principal components (PC).